ROYAL SOCIETY
OF CHEMISTRY

PAPER

Check for updates

Tunable-wavelength nanosecond laser tailoring of plasmon resonance spectra of gold nanoparticle colloids†

Thanyada Sukmanee, [ID] ‡ Michał Szuster,‡ Aleksander Gorski, [ID] Marcin Hołdyński and Sylwester Gawinkowski [ID] *

Metal nanoparticles have applications across a range of fields of science and industry. While there are numerous existing methods to facilitate their large-scale production, most face limitations, particularly in achieving reproducible processes and minimizing undesirable impurities. Common issues are varying particle sizes and aggregates with unfavorable spectral properties. Researchers are currently developing methods to separate or modify nanoparticle sizes and shapes post-synthesis and to eliminate impurities. One promising approach involves laser light irradiation and enables the changing of nanoparticle sizes and shapes while controlling crucial spectral parameters. In this work, we present a novel extension of this method by irradiating nanoparticle colloids with variable-wavelength nanosecond laser pulses on both sides of the extinction band. Our results demonstrate the use of gradual laser wavelength tuning to optimize the photothermal reshaping of gold nanorods and achieve precise control over the plasmon resonance band. By irradiating both sides of the plasmon resonance band, we execute a multistep tuning process, controlling the band's width and spectral position. A statistical analysis of SEM images reveals differences in the nanorod morphology when irradiated on the long- or short-wavelength side of the plasmon resonance band. The fine-tuning of plasmonic spectral properties is desirable for various applications, including the development of sensors and filters and the exploitation of the photothermal effect. The findings of this study can be extended to other plasmonic nanostructures.

Introduction

Gold nanoparticles have a wide range of applications across various fields, such as sensing,[1–4] imaging,[5,6] single-molecule detection,[7–9] optics,[10,11] catalysis,[12–14] biology,[5,15,16] and medicine.[17–19] As the demand for nanoparticle production continues to grow, it becomes essential to develop methods that guarantee high purity, accurate morphology, size, and property control, while also accommodating industrial-scale manufacturing capabilities. Gold nanoparticles possess unique optical properties resulting from the excitation of surface plasmon resonances (SPR), which are the collective oscillations of free electrons along metal lattices that allow them to capture and manipulate light efficiently at the nanoscale.[20,21] The SPR energy can be determined from optical extinction spectra and depends on various factors, such as the metal, the nanoparticle dimensions and shape, and the

dielectric properties of the environment.[22,23] Fine-tuning of the SPR and optimization for specific applications is possible by controlling these factors. However, obtaining large numbers of nanoparticles with the required optical properties can be challenging. Various protocols including chemical, photochemical, and electrochemical methods have been developed.[24–27] However, controlling these methods and ensuring reproducibility has proven challenging,[28] leading to significant by-products and nanoparticles with varying sizes, shapes, and aggregates. Moreover, the amount of each type of contamination, which causes a broadening of the SPR band, has also been found to vary between production batches, affecting reproducibility. The broadening of the SPR band could limit the feasibility of specific applications, as a precise match between the excitation and SPR wavelengths is often required for optimal performance. Furthermore, the localization of the electromagnetic field is much stronger in nanogaps formed in aggregates, which may dominate the spectral response of the colloid.[29–31]

Reproducing the optical properties of nanoparticles using chemical protocols is a significant obstacle to the widespread development and use of these materials. Therefore, post-production methods are being developed to improve the required properties of nanoparticles. Different methods of purification and separation have been devised.[32–35]

Institute of Physical Chemistry, Polish Academy of Sciences, Kasprzaka 44/52, 01-224 Warsaw, Poland. E-mail: sgawinkowski@ichf.edu.pl

† Electronic supplementary information (ESI) available: Description of the materials, experimental procedures, numerical analysis, and simulation procedures. See DOI: https://doi.org/10.1039/d3na00225j

‡ These authors contributed equally.

Alternatively, the optical properties of colloids can be improved through the modification of nanoparticles. One method that can be implemented even on a large scale is based on the pulsed laser irradiation of solutions of nanoparticles. Although still in its early stages, modification of nanoscale structures using ultra-short laser pulses has demonstrated considerable potential.[27,36–38]

In this study, we use laser light to photothermally reshape gold nanorod (GNR) colloids and precisely adjust their SPR bands. GNRs have two SPRs (Fig. 1), whose energies depend on the length and thickness of the rod.[39] The longitudinal SPR (LSPR) of a nanorod can be tuned over a broad range of energies, primarily by controlling the aspect ratio. Conversely, even minor changes in the aspect ratio result in significant shifts in the LSPR spectral position. Due to the challenge associated with maintaining precise control during synthesis, the resulting distribution leads to a substantial broadening of the LSPR. The width and position of the LSPR band can be influenced by irradiating a nanoparticle colloid with a laser beam. Pulsed lasers with femto- or nanosecond pulses are typically used to reshape nanoparticles and alter their SPRs,[36,40] although the utility of continuous-wave lasers has also been demonstrated.[41,42] The detailed reshaping mechanism depends on the duration and intensity of the laser pulse.[43–45] Generally, when nanoparticles are exposed to light tuned to the SPR frequency, their electrons oscillate collectively before thermalizing, which leads to local melting and atomic rearrangement within the nanoparticle.[46–48] However, using only one irradiation wavelength restricts the method's effectiveness, particularly when the SPR band is relatively broad. This process can be enhanced by employing a tunable wavelength laser and systematically adjusting it during irradiation. It has been shown that the SPR band of a nanorod colloid can be spectrally narrowed to almost the limit defined by the bandwidth of individual nanorods by applying femtosecond laser irradiation to the longer-wavelength side of the LSPR band.[38] Consequently, nanorods and aggregates with SPRs coinciding with applied laser wavelengths have been photothermally reshaped, and their SPRs shifted toward shorter wavelengths. By applying additional irradiations on the other side of the LSPR, it should also be feasible to affect this part of the band and control its position and width.

Building on this premise, we progressively altered the wavelength of a tunable nanosecond pulsed laser during such a process and applied it to both sides of the LSPR band. To our knowledge, this is the first report of short-wavelength side irradiation and its influence on the spectral response of the gold nanorods colloid. Furthermore, we are presenting double-sided irradiation of the LSPR band. This approach reduced the initially broad LSPR band below 80 nm for the partially-aggregated GNR colloid. We monitored the spectral changes and determined the final nanoparticle morphology using scanning electron microscopy (SEM). Additionally, we conducted a numerical analysis of the nanoparticle spectral and shape changes and verified the reproducibility of the procedure. Our post-synthesis refabrication method, which employs double-sided LSPR band irradiation, offers a straightforward alternative to complex chemical or separation techniques and can be used to prepare and develop novel plasmonic devices.

Experimental

Gold nanorod colloids were obtained through chemical synthesis using the seed growth method.[49] The resulting GNR colloids were characterized using SEM and extinction spectra analysis. Different batches of the synthesis produced slightly different size distributions of the GNRs and spectra, as shown in Fig. S4 of the ESI.† The colloids were irradiated in 1 cm quartz cuvettes equipped with a small magnetic stirring magnet driven by a home-built magnetic stirrer at 400 rpm. The Opotek Radiant SE 355 LD tunable wavelength nanosecond pulse laser was used to irradiate the colloids with a 5 ns pulse and 10 Hz repetition rate. The pulse energy was controlled with a gradient neutral density filter and set to 1 mJ before the cuvette. The irradiation time necessary for a slow but complete decrease of the extinction value at the irradiation wavelength was estimated at 30 minutes. Irradiation of the long-wavelength side of the LSPR band was initiated at the band's tail (830 nm) and gradually decreased to 680 nm in 10 nm steps. On the short-wavelength side of the LSPR band, the irradiation started at 600 nm and increased gradually in steps of 5 nm to 660 nm. After each irradiation step, the extinction spectrum of the colloid was measured using a Shimadzu UV-2700 spectrometer and 20 μl of the colloid was drop-casted onto a silicon substrate for SEM characterization. The SEM images were analyzed using custom Python code (details in ESI†) to extract statistical data.

Two-sided irradiation was conducted in a similar way to single-sided irradiation. Firstly, the long-wavelength side was irradiated starting at the tail of the LSPR band (830 nm) and gradually decreased to 750 nm in steps of 10 nm. Then, the irradiation on the short-wavelength side increased gradually in steps of 5 nm from 580 to 600 nm. The irradiation in each step lasted 30 minutes.

Results and discussion

Fig. 1 shows how the extinction spectra of the GNR colloids evolved with the separate irradiations on each side of the LSPR band. The band located at 515 nm represents the transverse SPR (TSPR) mode, while the broad band at 663 nm is the LSPR mode of the separate GNRs and their aggregates. The LSPR band is more prone to changes due to laser-induced variations in the aspect ratios of nanorods and their size dispersion.[4,50] The irradiation process started at the long-wavelength tail of the LSPR band and the spectral changes of the colloid were monitored. As the extinction at the irradiation wavelength dropped close to zero, the irradiation wavelength gradually changed. The subsequent irradiations were closer to the maximum of the LSPR band and typically led to a narrower full width at half maximum (FWHM), decreasing it from 165 to 100 nm (Fig. 1(e)). A gradual reduction in intensity on the longer-wavelength side of the LSPR band shapes its towards a Lorentzian profile. However, concurrently on the other side of the band, an increase in intensity is observed, resulting in only a moderate
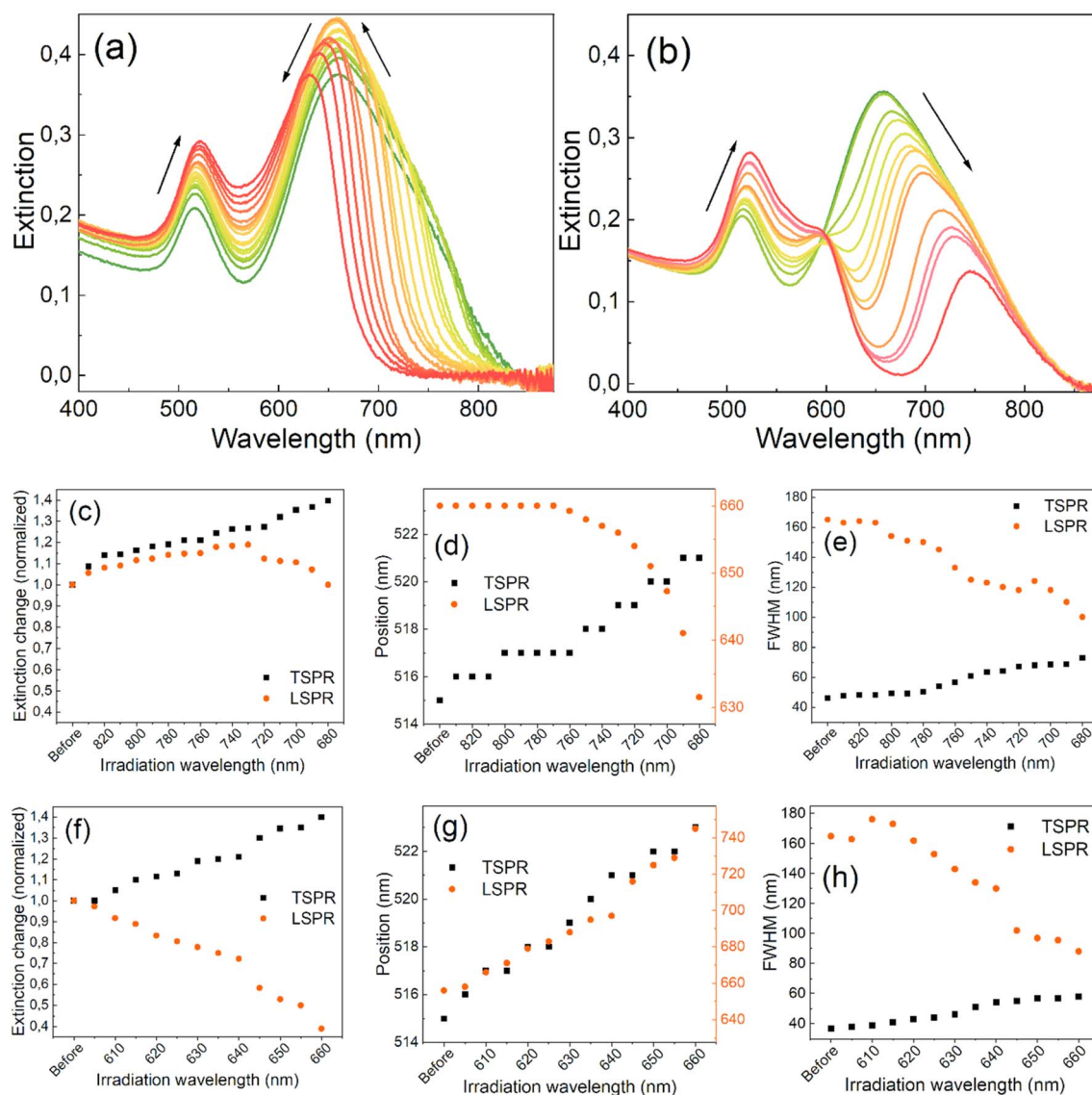
Fig. 1 The evolution of the extinction spectra of the GNR colloid during irradiation on the longer- (a) and shorter- (b) wavelength side of the LSPR band. The consecutive irradiation starts with the green curve and ends with the red curve. The arrows indicate the directions of changes. Parts (c) through (h) show the evolution of specific spectral parameters during the irradiation procedure: extinction (c and f), peak position (d and g), and FWHM (e and h), for longer- and shorter-wavelength LSPR band side irradiations, respectively.

decrease in its FWHM. Consequently, when the wavelength of irradiation closely approaches the original peak position of the band, the peak also begins to shift towards shorter wavelengths. The changes in the extinction values and the positions of the SPR bands are depicted in Fig. 1(a)–(f).

Irradiating the LSPR band on either side results in an increase in the extinction of the TSPR band. Fig. 1(c) shows that when irradiated on the longer-wavelength side of the LSPR band, the extinction of the LSPR initially increases by around 20% in the first few steps but then starts to decrease with each subsequent irradiation. In contrast, the extinction of the LSPR decreases almost immediately from the beginning of the irradiation started on the shorter-wavelength side of the band (Fig. 1(b)). The position of the maximum of the LSPR band

remains constant at the beginning of the long-wavelength-side irradiation but starts to quickly blue-shift at the same point when the intensity of the band begins to decrease (Fig. 1(d)). On the other hand, the intensity of the TSPR band continuously increases and red-shifts throughout the entire procedure, regardless of the irradiation side (Fig. 1(d) and (g)). In both cases, the FWHMs of the LSPRs continuously decrease while the FWHMs of the TSPRs increase (Fig. 1(e) and (h)).

These results suggest the reshaping of the nanorods, resulting in an increased population of shorter nanorods and their thickening, as has been observed in other studies.[37,51,52] They also suggest the elimination of aggregates, which have a longer-wavelength SPR band than separated nanorods. When irradiated from the longer-wavelength side, the maximum

extinction intensity of the LSPR band is reached when the irradiation wavelength goes down to 730 nm, suggesting that the entire irradiation process should be stopped at this point. However, further narrowing of the band requires continuing the irradiation process at the cost of slightly lower extinction.

When irradiated from the shorter-wavelength side of the LSPR band, the band peak position shifts and systematically narrows while the band loses its intensity (Fig. 1(f)–(h)). This irradiation mainly decreases the population of short nanorods in the colloid, converting them into more spherically-shaped nanoparticles. The energy of the laser pulses was tested and maintained at a level that induced slow spectral changes throughout the entire process. Higher laser pulse energies result in the re-ablation of nanoparticles and do not permit the precise control of outcomes, leading to the fragmentation and creation of nanoparticles of varying sizes. Maintaining the laser pulse energy below the threshold required for nanoparticle ablation allows for better control of the process and its results. Under such conditions, structural changes in the nanoparticles occur due to the melting or thermal reshaping of the irradiated nanorods, which have the same resonance as the laser wavelength irradiation.[46,53]

The statistical analysis of the SEM images confirmed the absence of fragmentation of nanoparticles (see ESI†). The transformation of extinction spectra due to laser irradiation results from changes in the size, shape, and population dispersity of nanoparticles in the colloid. Fig. 2 presents SEM images of nanorod colloids before and after irradiation. Initially, the nanorods in Fig. 2(a) and (c) were predominantly regular rod-shaped particles. Fig. 2(b) shows nanorods with shorter lengths and more spheroidal shapes resulting from irradiation on the long-wavelength (830–680 nm) side of the LSPR band. Fig. 2(d) reveals more irregular forms when the nanorods are irradiated on the short-wavelength (600–660 nm) side.

The observed changes in the spectra can be attributed to the reshaping of nanorods with different LSPRs under irradiation with different wavelengths. Specifically, when irradiated at the longer-wavelength tail of the LSPR band, only the longest GNRs and aggregates with LSPRs shifted toward longer wavelengths are affected. As the laser is shifted to a slightly shorter wavelength, it becomes better tuned to the SPRs of other populations of nanorods. Due to the photothermal effect, those nanorods change shape and adopt a more spheroidal morphology (Fig. 2) with LSPRs at shorter wavelengths. Such morphological changes are very similar to previously reported for the GNRs colloids irradiated with femtosecond pulses[38,51] and single dry nanorods irradiated under microscope.[37,46] The photothermal mechanism of laser-induced morphology changes may be supported by the results of experiments using solely thermal means, which show the same shape changes.[54] The progressive spheroidization of the GNRs is confirmed by the systematic changes in the population of nanorods with different aspect ratios (Fig. 3). The additional extinction of reshaped GNRs contributes to the extinction intensity of the remaining unaffected GNRs, leading to a local increase in the LSPR band intensity. This may also cause a shift in its maximum (Fig. 4). Conversely, when irradiated at the shorter-wavelength side of the LSPR, the resulting more spheroidal nanoparticles have LSPR resonances shifted even further toward the original
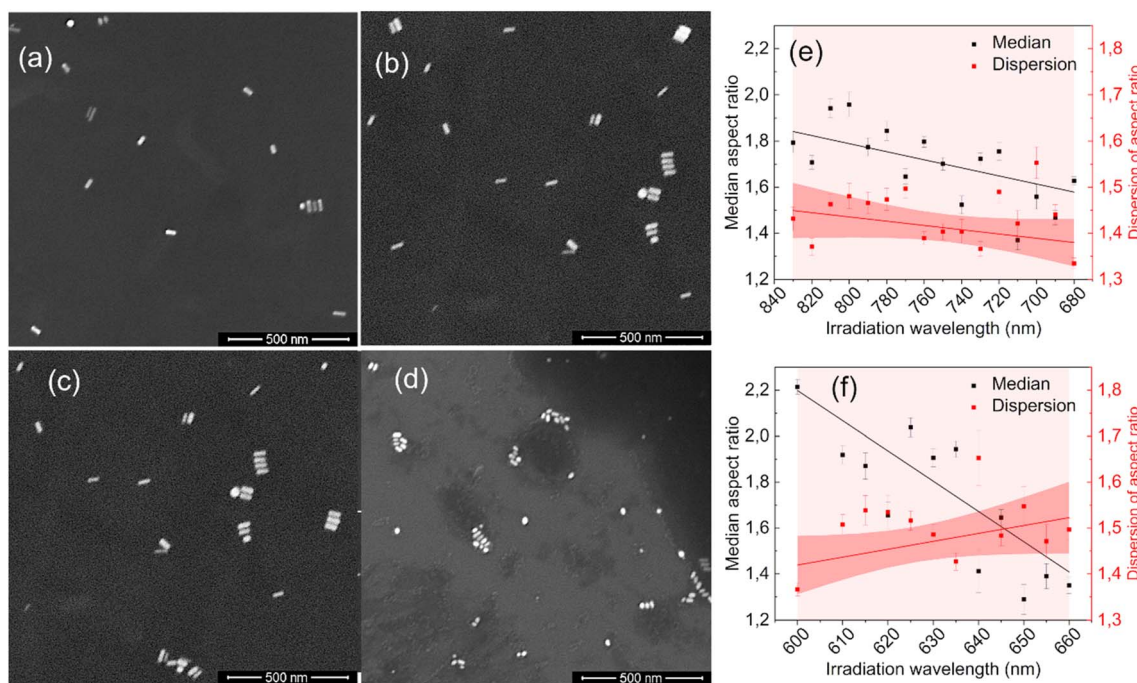

Fig. 2 SEM images of GNRs before irradiation (a and c) and after irradiation on the longer- (b) and shorter- (d) wavelength sides of the LSPR band. Changes in the median and dispersion of the aspect ratio distribution of GNRs observed after irradiation on the longer- (e) and shorter- (f) wavelength side of the LSPR band. The red shadows show 95% confidence intervals.
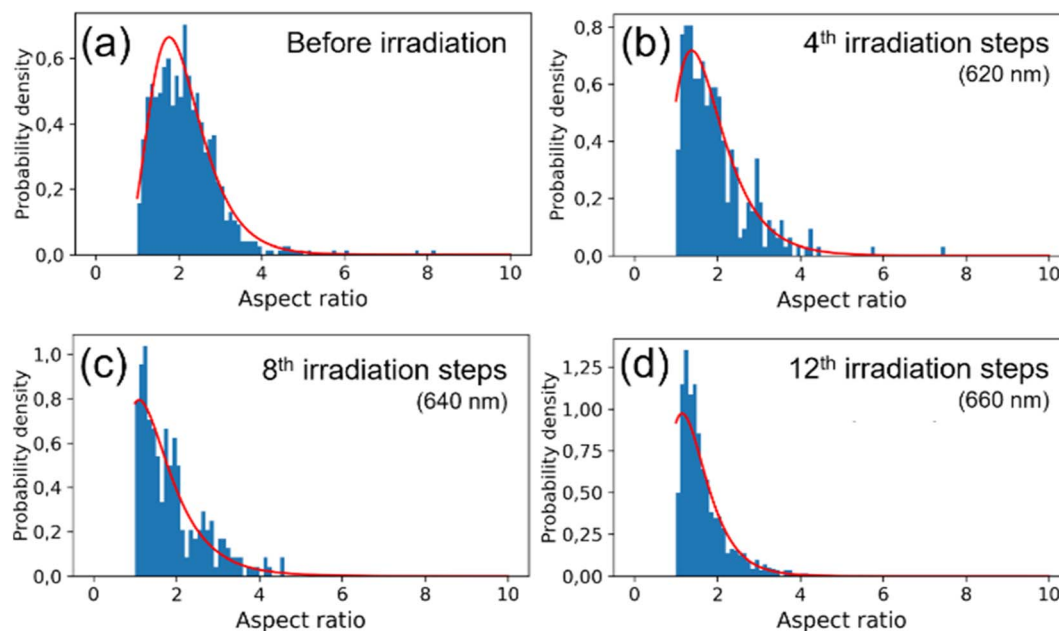
Fig. 3 Histograms showing the aspect ratio obtained from SEM images before (a) and after irradiation steps 4 (b), 8 (c), and 12 (d) on the shorter-wavelength side of the LSPR band. The red curve represents a fitted modified lognormal distribution.

transverse surface plasmon resonance (TSPR), causing only a decrease in the local intensity of the LSPR. The decreasing aspect ratio of the nanorods is also a result of their thickening. As the transverse dimension of the GNRs is not controlled during the irradiation process, it results in a larger variation in the transverse dimension for the whole population of nanoparticles. This causes a broadening of the TSPR band on the extinction spectrum. Thicker nanorods have a plasmon resonance at slightly lower energies and are more intense, so the TSPR band appears shifted toward longer wavelengths and is slightly higher.

Visual inspection of the SEM images only allows for the identification of significant changes in the morphology of the GNRs, such as those before and after all irradiation steps (Fig. 2(a)–(d)). We conducted a numerical analysis (see ESI†) to analyze these changes further. For each irradiation step, we selected at least a few hundred GNRs to ensure an accurate representation of the results. The aspect ratio of the long to short dimensions was used to parameterize the morphological changes. The accuracy of the representation of the GNRs as ellipsoids was tested by using the populations of ellipsoidal nanoparticles extracted numerically from the SEM images as input for simulating their absorption spectra (see ESI†). The simulated spectra of populations of ellipsoidal gold nanoparticles showed qualitative similarity to the experimentally-measured extinction spectra of GNR colloids from which the SEM samples were taken (Fig. S3 in ESI†). The analysis revealed variations in the median and dispersion of the aspect ratio due to irradiation. The aspect ratios of the GNRs decreased gradually with irradiation on either side of the LSPR band (Fig. 2(e) and (f)). However, the dispersion of the aspect ratios decreased when the colloid was irradiated on the longer-wavelength side
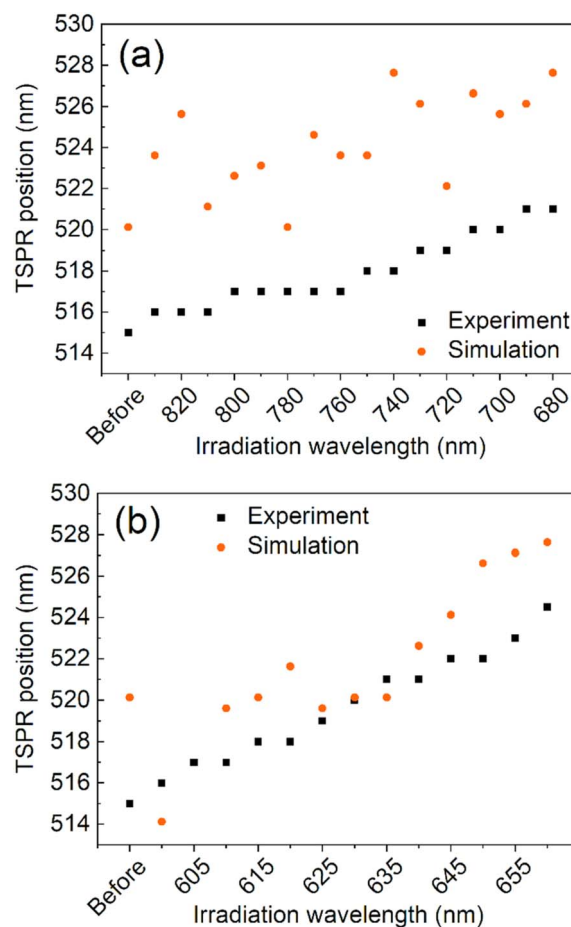

Fig. 4 A comparison between simulation and experiment for the maximum wavelength of the TSPR band for the long- (a) and short-wavelength (b) sides of the LSPR irradiation processes, respectively.

of the LSPR band but increased with irradiation on the shorter-wavelength side. It is worth noting that the change in the dispersion was minor in both cases. These results suggest that the main factor responsible for changes in the SPR bands due to irradiation was the change in the aspect ratio of the GNRs.

The reproducibility of the results was tested using different batches of GNR colloids obtained by direct chemical synthesis. The results for initially significantly different colloidal solutions (Fig. S4 in the ESI†) are presented in Fig. S5–S7 in the ESI.† The later sample has a narrower distribution of GNR sizes, resulting in a narrower initial range of the LSPR band (an FWHM of 122 nm). A similar irradiation process was applied to it as for the first sample, except for slightly different laser wavelength ranges. The induced changes in the spectral parameters of the TSPR band were also similar (Fig. S6 in the ESI†). The LSPR band narrowed to 72 nm for irradiation on the longer-wavelength side of the LSPR band. Statistical analysis of SEM images of nanorods from these irradiations revealed similar morphological changes in the GNRs, as shown by the median and dispersion of the length-to-width ratios and the TSPR band positions during the procedure (Fig. S7 and S8 in the ESI†).

We have demonstrated that by gradually shifting the irradiation wavelength on one side of the LSPR, we can significantly alter the optical properties of nanorod colloids and achieve a high degree of control over the final FWHM and its spectral position. In order to further investigate the potential of this method for tailoring the LSPR band and minimizing inhomogeneous spectral broadening, we conducted an experiment to determine if consecutive irradiations on both sides of the LSPR could further improve the shape of the LSPR band. The results of this experiment are presented in Fig. 5. Two-sided irradiation was systematically performed using laser excitations at 830–750 nm and 580–600 nm. These irradiation ranges were dictated by the additional goal of holding the LSPR band position at 665 nm, close to the original position of its maximum. The outcome showed that the LSPR bandwidth decreased to 80 nm after irradiation on both sides. This result is comparable to the FWHM obtained with the chemical method[55] and close to the boundary range expected for a single GNR,[56] taking into account significant variation of shapes. This value of FWHM is similar to that achieved for irradiation on only one side, but in this case the extinction intensity at the maximum was almost unaffected. This also led to a more symmetrical shape of the LSPR band.

Conclusions

This study has presented a novel method to improve the shape and control the position of the LSPR band maximum while altering the optical properties of colloidal GNR solutions by gradually adjusting the laser wavelength. For the first time, the irradiation has been applied to both short- and long-wavelength sides of the LSPR band to control the shape and position of the LSPR band. Gradual tuning of the laser wavelength is crucial for inducing photothermal changes in GNRs in a controlled manner. The spectral changes resulting from the irradiation are due to the reshaping of the GNRs and the changes in their aspect ratios. Irradiation on the long-wavelength side of the LSPR band reduces the bandwidth by shortening the length of longer GNRs and eliminating their aggregates while allowing for a relatively wide range of peak position adjustments. In contrast, irradiation on the short-wavelength side of the LSPR band also narrows the plasmon band, but the spectral range of the peak position adjustment is much smaller, and the band remains highly asymmetric.

Optimal control of the LSPR peak shape was achieved by applying repeated irradiations to both sides of the LSPR peak. This approach was found to maintain the maximum optical density while achieving an FWHM close to the limit of a single GNR, leading to better control of the SPR bands. Improved control of the LSPR peak shape and position can significantly enhance the applicability of GNRs in various fields, including sensor and filter development and photothermal applications such as phototherapy, photothermal heating, and photothermal cleaning.
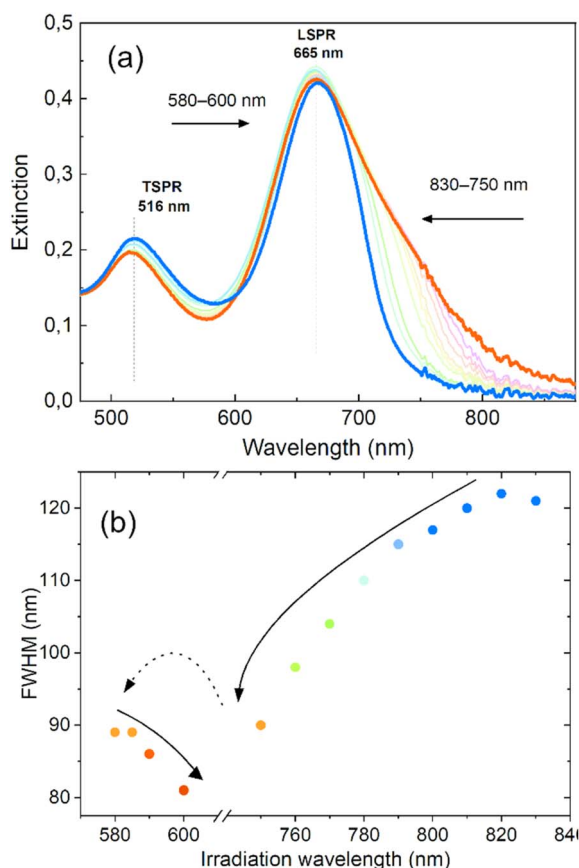

Fig. 5 The evolution of the extinction spectra of the GNR colloid due to irradiation on both sides of the LSPR band (a). The red and blue curves represent spectra before and after all irradiations, and the arrows indicate the directions of the changes. The FWHM evolution due to irradiation (b).

Data availability

The data supporting this research is stored in the Repod repository and is available at **https://doi.org/10.18150/L0AR5F**.

Author contributions

Conceptualization, S. G.; investigation, T. S., M. Sz., A. G., M. H., and S. G.; methodology, S. G. and M. Sz.; software, M. Sz.; writing – original Draft preparation, M. Sz. and T. S.; writing – review & editing, S. G. and T. S.; supervision, S. G.; funding acquisition, S. G.

Conflicts of interest

There are no conflicts to declare.

Acknowledgements

References

1 N. H. Anh, M. Q. Doan, N. X. Dinh, T. Q. Huy, D. Q. Tri, L. T. N. Loan, B. V. Hao and A.-T. Le, *RSC Adv.*, 2022, **12**, 10950–10988.

2 K. Saha, S. S. Agasti, C. Kim, X. Li and V. M. Rotello, *Chem. Rev.*, 2012, **112**, 2739–2779.

3 G. Yue, S. Su, N. Li, M. Shuai, X. Lai, D. Astruc and P. Zhao, *Coord. Chem. Rev.*, 2016, **311**, 75–84.

4 J. Cao, T. Sun and K. T. V. Grattan, *Sens. Actuators, B*, 2014, **195**, 332–351.

5 Y.-S. Chen, Y. Zhao, S. J. Yoon, S. S. Gambhir and S. Emelianov, *Nat. Nanotechnol.*, 2019, **14**, 465–472.

6 M. Bouché, J. C. Hsu, Y. C. Dong, J. Kim, K. Taing and D. P. Cormode, *Bioconjugate Chem.*, 2020, **31**, 303–314.

7 S. Nie and S. R. Emory, *Science*, 1997, **275**, 1102–1106.

8 M. Pszona, S. Gawinkowski, R. Jäger, I. Kamińska and J. Waluk, *J. Chem. Phys.*, 2022, **156**, 014201.

9 A. B. Zrimsek, N. Chiang, M. Mattei, S. Zaleski, M. O. McAnally, C. T. Chapman, A.-I. Henry, G. C. Schatz and R. P. Van Duyne, *Chem. Rev.*, 2017, **117**, 7583–7613.

10 M. O. Stetsenko, S. P. Rudenko, L. S. Maksimenko, B. K. Serdega, O. Pluchery and S. V. Snegir, *Nanoscale Res. Lett.*, 2017, **12**, 1–10.

11 D. Wang, J. Li, C. T. Chan, V. Salgueiriño-Maceira, L. M. Liz-Marzán, S. Romanov and F. Caruso, *Small*, 2005, **1**, 122–130.

12 T. Ishida, T. Murayama, A. Taketoshi and M. Haruta, *Chem. Rev.*, 2020, **120**, 464–525.

13 H. Wang, L. Wang, D. Lin, X. Feng, Y. Niu, B. Zhang and F.-S. Xiao, *Nat. Catal.*, 2021, **4**, 418–424.

14 J. Aizpurua, J. Baumberg, V. Caps, E. Cortes, B. de Nijs, Y. D. Fernandez, L. Fabris, S. Freakley, S. Gawinkowski, D. Glass, J. Huang, B. Jankiewicz, J. Khurgin, P. V. Kumar, R. J. Maurer, P. McBreen, N. S. Mueller, J. Y. Park, J. Quiroz, S. Rejman, R. M. R. Gómez, J. Salmon-Gamboa, S. Schlücker, Z. Schultz, A. Shukla, Y. Sivan, M. Thangamuthu, L. Torrente-Murciano, X. Xiao, H. Xu and C. Zhan, *Faraday Discuss.*, 2019, **214**, 479–499.

15 N. Lippok, M. Villiger, A. Albanese, E. F. J. Meijer, K. Chung, T. P. Padera, S. N. Bhatia and B. E. Bouma, *Nat. Photonics*, 2017, **11**, 583–588.

16 I. Fratoddi, I. Venditti, C. Cametti and M. V. Russo, *Nano Res.*, 2015, **8**, 1771–1799.

17 L. A. Dykman and N. G. Khlebtsov, *Biomed. Opt. Express*, 2019, **10**, 3152–3182.

18 H. Arami, S. Kananian, L. Khalifehzadeh, C. B. Patel, E. Chang, Y. Tanabe, Y. Zeng, S. J. Madsen, M. J. Mandella, A. Natarajan, E. E. Peterson, R. Sinclair, A. S. Y. Poon and S. S. Gambhir, *Nat. Nanotechnol.*, 2022, **17**, 1015–1022.

19 J. Ye, Q. Wen, Y. Wu, Q. Fu, X. Zhang, J. Wang, S. Gao and J. Song, *Nano Res.*, 2022, **15**, 6372–6398.

20 L. Novotny and N. van Hulst, *Nat. Photonics*, 2011, **5**, 83–90.

21 M. I. Stockman, K. Kneipp, S. I. Bozhevolnyi, S. Saha, A. Dutta, J. Ndukaife, N. Kinsey, H. Reddy, U. Guler, V. M. Shalaev, A. Boltasseva, B. Gholipour, H. N. S. Krishnamoorthy, K. F. MacDonald, C. Soci, N. I. Zheludev, V. Savinov, R. Singh, P. Groß, C. Lienau, M. Vadai, M. L. Solomon, D. R. Barton, M. Lawrence, J. A. Dionne, S. V. Boriskina, R. Esteban, J. Aizpurua, X. Zhang, S. Yang, D. Wang, W. Wang, T. W. Odom, N. Accanto, P. M. de Roque, I. M. Hancu, L. Piatkowski, N. F. van Hulst and M. F. Kling, *J. Opt.*, 2018, **20**, 043001.

22 S. A. Maier, *Plasmonics: Fundamentals and Applications*, New York, NY, 2010.

23 *Optical Antennas*, ed. M. Agio and A. Alù, Cambridge University Press, Cambridge, Illustrated edition, 2013.

24 C. Daruich De Souza, B. Ribeiro Nogueira and M. E. C. M. Rostelato, *J. Alloys Compd.*, 2019, **798**, 714–740.

25 R. Herizchi, E. Abbasi, M. Milani and A. Akbarzadeh, *Artif. Cells, Nanomed., Biotechnol.*, 2016, **44**, 596–602.

26 H. Zeng, X.-W. Du, S. C. Singh, S. A. Kulinich, S. Yang, J. He and W. Cai, *Adv. Funct. Mater.*, 2012, **22**, 1333–1353.

27 D. Zhang, B. Gökce and S. Barcikowski, *Chem. Rev.*, 2017, **117**, 3990–4103.

28 R. Gallagher, X. Zhang, A. Altomare, D. Lawrence, N. Shawver, N. Tran, M. Beazley and G. Chen, *Nano Res.*, 2021, **14**, 1167–1174.

29 B. Vlčková, X. J. Gu and M. Moskovits, *J. Phys. Chem. B*, 1997, **101**, 1588–1593.

30 I. W. Sztainbuch, *J. Chem. Phys.*, 2006, **125**, 124707.

31 K. Faulds, R. E. Littleford, D. Graham, G. Dent and W. E. Smith, *Anal. Chem.*, 2004, **76**, 592–598.

32 Á. I. López-Lorente and M. Valcárcel, in *Comprehensive Analytical Chemistry*, ed. M. Valcárcel and Á. I. López-Lorente, Elsevier, 2014, vol. 66, pp. 357–394.

33 S. F. Sweeney, G. H. Woehrle and J. E. Hutchison, *J. Am. Chem. Soc.*, 2006, **128**, 3190–3197.

34 G. Chen, Y. Wang, L. H. Tan, M. Yang, L. S. Tan, Y. Chen and H. Chen, *J. Am. Chem. Soc.*, 2009, **131**, 4218–4219.

35 J. D. Robertson, L. Rizzello, M. Avila-Olias, J. Gaitzsch, C. Contini, M. S. Magoń, S. A. Renshaw and G. Battaglia, *Sci. Rep.*, 2016, **6**, 27494.

36 G. González-Rubio, A. Guerrero-Martínez and L. M. Liz-Marzán, *Acc. Chem. Res.*, 2016, **49**, 678–686.

37 M. Gordel, J. Olesiak-Banska, K. Matczyszyn, C. Nogues, M. Buckle and M. Samoc, *Phys. Chem. Chem. Phys.*, 2013, **16**, 71–78.

38 G. González-Rubio, P. Díaz-Núñez, A. Rivera, A. Prada, G. Tardajos, J. González-Izquierdo, L. Bañares, P. Llombart, L. G. Macdowell, M. Alcolea Palafox, L. M. Liz-Marzán, O. Peña-Rodríguez and A. Guerrero-Martínez, *Science*, 2017, **358**, 640–644.

39 J. Zheng, X. Cheng, H. Zhang, X. Bai, R. Ai, L. Shao and J. Wang, *Chem. Rev.*, 2021, **121**, 13342–13453.

40 S. Link, C. Burda, B. Nikoobakht and M. A. El-Sayed, *J. Phys. Chem. B*, 2000, **104**, 6152–6163.

41 K. Setoura, Y. Okada and S. Hashimoto, *Phys. Chem. Chem. Phys.*, 2014, **16**, 26938–26945.

42 D. Harris-Birtill, M. Singh, Y. Zhou, A. Shah, P. Ruenraroengsak, M. E. Gallina, G. B. Hanna, A. E. G. Cass, A. E. Porter, J. Bamber and D. S. Elson, *PLoS One*, 2017, **12**, e0185990.

43 S. Link, C. Burda, M. B. Mohamed, B. Nikoobakht and M. A. El-Sayed, *J. Phys. Chem. A*, 1999, **103**, 1165–1170.

44 T. E. Itina, *J. Phys. Chem. C*, 2011, **115**, 5044–5048.

45 É. Boulais, R. Lachaine and M. Meunier, *J. Phys. Chem. C*, 2013, **117**, 9386–9396.

46 A. B. Taylor, A. M. Siddiquee and J. W. M. Chon, *ACS Nano*, 2014, **8**, 12071–12079.

47 Y. Mansour, Y. Battie, A. E. Naciri and N. Chaoui, *Nanoscale*, 2019, **11**, 11679–11686.

48 J. Yan, D. Zhu, J. Xie, Y. Shao and W. Xiao, *Small*, 2020, **16**, 2001101.

49 B. Nikoobakht and M. A. El-Sayed, *Chem. Mater.*, 2003, **15**, 1957–1962.

50 V. Sharma, K. Park and M. Srinivasarao, *Mater. Sci. Eng., R*, 2009, **65**, 1–38.

51 P. Díaz-Núñez, G. González-Rubio, A. Prada, J. González Izquierdo, A. Rivera, L. Bañares, A. Guerrero-Martínez and O. Peña-Rodríguez, *J. Phys. Chem. C*, 2018, **122**, 19816–19822.

52 M. Censabella, M. G. Grimaldi and F. Ruffino, *Mater. Charact.*, 2019, **147**, 101–115.

53 X. Hou, N. Djellali and B. Palpant, *ACS Photonics*, 2018, **5**, 3856–3863.

54 H. Cho, J. W. Shin and R. Ryoo, *J. Phys. Chem. C*, 2020, **124**, 12855–12863.

55 B. P. Khanal and E. R. Zubarev, *Chem.–Eur. J.*, 2019, **25**, 1595–1600.

56 M. Hu, C. Novo, A. Funston, H. Wang, H. Staleva, S. Zou, P. Mulvaney, Y. Xia and G. V. Hartland, *J. Mater. Chem.*, 2008, **18**, 1949–1960.